Medical Drill Wear Classification Using Servomotor Drive Signals and Neural Networks

Tomislav Staroveski, Danko Brezak, Vinko Grdan, and Tomislav Bacek

Abstract— **Medical drills are subject to intensive wear due to the influence of different mechanical, chemical and thermal factors characteristic for drilling and sterilization process. Wear progress increases friction in the cutting zone, which consequently leads to higher temperatures and cutting forces, i.e., possible thermal and mechanical damages of the bone tissue. Therefore, the presented study aimed to analyze the possibility of drill wear monitoring using electric servomotor drive signals and neural network algorithm. Experimental work has been performed with adequately designed testbed machining system and using prepared bovine bone samples. Drill wear features were extracted from time and frequency domain of the process signals, and then analyzed separately and in combinations.**

Index Terms—**medical drill, wear, thermal osteonecrosis, neural networks, modeling**

I. Introduction

ALL orthopedic, trauma or dental bone drilling interventions consequently imply heat generation that can significantly influence the treatment quality and postoperative recovery process. Although its mechanisms are not fully depicted, it is a known fact that temperature rise leads to bone tissue damages or thermal osteonecrosis [1, 2]. One of the most influential factors with high impact on heat generation during bone drilling is drill wear. Drill wear is unavoidable and irreversible process which increases friction and tool vibrations, thus resulting in higher cutting forces and drilling temperature. Except thermal damages, tool wear process can also cause mechanical bone damages as a result of cutting edge fracture or complete tool breakage.

Medical drills wear out due to the mechanical, chemical and thermal factors which occur during sterilization and continuous application in different cutting conditions (bone density, cooling type, drill material and geometry, etc.). Several studies point out to the strong and proportional relationship between drilling temperature rise and tool wear process dynamics or drill cutting edges condition [3-6]. At the same time, some researchers also emphasized the frequent usage of worn drills in medical interventions, as well as absence of hospital standards and activities focused to drill wear identification and tool labeling [7].

It is therefore logically to presume that precise and reliable drill wear models could become important tool in reducing a possibility of bone tissue damages, thus enabling faster postoperative treatment progress. Their role is particularly important in the development of completely automated medical drilling systems.

The width of flank wear (VB), which is the most common tool wear parameter, cannot be measured during the drilling process, but only estimated using tool wear features extracted from the process signals and other known machining parameters (cutting speed, feed rate, drill characteristics). Although several models for temperature estimation have been proposed [8, 9], none of them includes drill wear estimation. Moreover, to our knowledge, there are still no tool wear monitoring solutions specifically designed for medical applications, or experimental studies based on the application of some of already designed and tested industrial solutions in bone drilling.

Tool wear dynamics has been shown as highly nonlinear and partially stochastic in industrial applications [10]. Similar characteristics can be expected in bone drilling due to the complex bone structure. Complexity of wear process in industrial applications motivated many researchers to use different types of computational intelligence algorithms, primarily artificial neural networks, to build reliable and accurate wear models. One of their main advantages is the capability of nonlinear system/process modeling based on parallel processing and integration of large amount of data, or, in this case, tool wear features extracted from the measured process signals.

The aim of this study was to analyze the applicability of tool wear features extracted from only servomotor drives current signals in drill wear level classification. This approach was chosen from the aspect of the fastest potential implementation of a drill wear monitoring system in the existing hand-held medical drilling machines. Based on chosen tool wear features, which were extracted from time and frequency domain, neural network model was tested in order to see how well it can classify worn from sharp drill. For this purpose, a type of Radial Basis Function Neural Network (RBF NN) algorithm for dealing with classification types of problems has been chosen. This NN is known for its learning in one step and a capability of simple and quick hidden layer structure adaptation.

Manuscript received December 30, 2013; revised February 5, 2014. This work was supported by the Ministry of Science, Education and Sport of the Republic of Croatia through fund for national scientific projects.

T. Staroveski is with the Faculty of Mechanical Engineering and Naval Architecture, University of Zagreb, Croatia (e-mail: tstaroveski@fsb.hr).

D. Brezak is with the Faculty of Mechanical Engineering and Naval Architecture, University of Zagreb, Croatia (phone: +385 1 6168357, fax: +385 1 6168351; e-mail: danko.brezak@fsb.hr).

V. Grdan is with the Faculty of Mechanical Engineering and Naval Architecture, University of Zagreb (e-mail: vinko747@hotmail.com).

T. Bacek is with the Faculty of Mechanical Engineering and Naval Architecture, University of Zagreb (e-mail: tomislav.bacek@fsb.hr).

ISBN: 978-988-19252-7-5
ISSN: 2078-0958 (Print); ISSN: 2078-0966 (Online)

II. RBF Neural Network Algorithm

Utilized NN algorithm is based upon a well-known feedforward three-layered RBF NN architecture, where the matrix/vector of synaptic weights $\boldsymbol{c}$ is calculated in the learning phase using the expression

$$\boldsymbol{c} = \boldsymbol{H}^{+}\boldsymbol{y}, \tag{1}$$

where $\boldsymbol{y}$ stands for the matrix/vector of desired output values and $\boldsymbol{H}^{+}$ is Moore – Penrose pseudoinverse of the matrix of hidden layer neuron RBF outputs or activation function outputs ($\boldsymbol{H}$). The pseudoinverse is defined as follows

$$\boldsymbol{H}^{+} = \left(\boldsymbol{H}^{T}\boldsymbol{H}\right)^{-1}\boldsymbol{H}^{T}. \tag{2}$$

In the testing phase, the matrix of desired output values $\boldsymbol{y}$ is obtained from the expression

$$\boldsymbol{y} = \boldsymbol{H}\boldsymbol{c}. \tag{3}$$

Elements of matrix $\boldsymbol{H}$ are determined according to the expression [11]

$$H_{ij} = e^{-\frac{1}{2}r_{ij}^{2}},\ i = 1,\ ...,\ N,\ j = 1,\ ...,\ K, \tag{4}$$

where r_{ij} is the Mahalanobis distance between vector composed from ith element of all input vectors (tool wear features) and jth hidden layer neuron. Squared Mahalanobis distance is calculated using the expression

$$r_{ij}^{2} = \left(\boldsymbol{x}_i - \boldsymbol{t}_j\right)^{T}\boldsymbol{\Sigma}_j^{-1}\left(\boldsymbol{x}_i - \boldsymbol{t}_j\right), \tag{5}$$

where $\boldsymbol{\Sigma}_j$ is a covariance matrix belonging to the group of learning samples that are connected to the jth hidden layer neuron, $\boldsymbol{x}_i$ is the L-dimensional vector composed from ith element of all L input vectors and $\boldsymbol{t}_j$ is L-dimensional vector of the jth hidden layer neuron center. Covariance matrix is quadratic matrix with non-zero elements (squared $\boldsymbol{\sigma}$ vector components) on main diagonal and zeros elsewhere,

$$\boldsymbol{\Sigma}_j = \begin{bmatrix} \sigma_1^{2} & 0 & 0 \\ 0 & \ddots & 0 \\ 0 & 0 & \sigma_L^{2} \end{bmatrix}. \tag{6}$$

Vector $\boldsymbol{\sigma}$ is composed from the maximal Euclidian distances between learning samples belonging to the analyzed group and the center of that group, regarding to all (L) dimensions separately,

$$\sigma_g|_j = max\left\{\left\| z_{pg} - t_g \right\|,\ p = 1,...,LK_G\right\}|_j,\ g = 1,...,L, \tag{7}$$

where z_{pg} is the gth component of the pth sample of the jth group which is defined with LK_G numbers of samples, and t_g is gth component of the jth group center vector (jth hidden layer neuron center vector).

Hidden layer neuron centers are determined using a method which helps teacher to quickly determine the network structure regarding to the nature of the learning problem and desirable generalization characteristics.

A. Hidden Layer Structure Configuration

Tool wear features (elements) grouping and centers calculations are based on the parameter β_C. In the first phase, the initial β_C parameter value needs to be established. It can be determined by using the following algorithm:

1) A referent element (*RE*) has to be defined first. Any input vector $\boldsymbol{x}_i$ used in the learning phase can be set as *RE*. Other combinations are also possible. For example, in this work, *RE* is calculated on the basis of the minimal values of all classification features,

$$RE(g) = min\left(\boldsymbol{x}_g\right),\ g = 1,...,L, \tag{8}$$

where $\boldsymbol{x}_g$ is the gth L-dimensional input vector;

2) From the referent element and its surrounding elements (10 nearest elements were chosen) a referent group can be established. Surrounding elements are determined by calculating the minimal Euclidian distances between *RE* and all elements of the learning space;
3) Finally, the initial β_C parameter value calculates from equation (9) as a mean value of the Euclidian distances between nearest neighborhood elements of the referent group,

$$\beta_C = \frac{\sum_{p=1}^{L_G} min\left\{\left\| u_p - u_m \right\|,\ m = 1,...,L_G\ ,\ \ p \neq m\right\}}{L_G}, \tag{9}$$

where u is L-dimensional vector composed from the referent group elements, and L_G represents the number of the referent group elements (L_G=10).

Based on the initial β_C parameter value and its subsequent empirical adaptations it is possible to determine the hidden layer neuron centers number and their values. Centers determination algorithm is divided in six steps, and it needs to be carried out for all classes separately.

1) The first learning element of the considered class is taken for the center of the first considered group.
2) The center is compared with all elements of the same class by calculating their Euclidian distances.
3) If the distance does not exceed β_C parameter value the element is ranged in the group belonging to the considered center. Otherwise, the element stays out of the group.
4) After the analysis of all distances, the new center is calculating as a mean value of all elements of the considered group.
5) The algorithm continues from the 2nd step for the new center value, and after the 4th step the center of the considered group is determined.
6) Elements which have been grouped are excluded from further calculations, and the next ungrouped element is

ISBN: 978-988-19252-7-5
ISSN: 2078-0958 (Print); ISSN: 2078-0966 (Online)

taken for the initial center of the next group. The algorithm continues from the 2nd step.

By changing only one (β_C) parameter, this algorithm provides fast modifications of hidden layer structure in order to achieve required generalization characteristics of the RBF NN.

III. Experimental Setup, Signal Processing and Features Extraction

A. Experimental Setup

Experimental work has been performed using the 3-axis bench-top mini milling machine adjusted for the purpose of bone drilling research (Fig. 1). The machine has been retrofitted with the 0.4 kW (1.27 Nm) permanent magnet synchronous motors with integrated incremental encoders (type Mecapion SB04A), corresponding motor controllers (DPCANIE-030A400 and DPCANIE-060A400), ball screw assemblies, and LinuxCNC open architecture control (OAC) system. Two types of signals were sampled from those controllers: vertical or Z-axis feed drive current (I_Z) and main spindle current (I_{MS}).

For the purpose of this study, cutting forces have also been measured using Kistler piezoelectric dynamometer 9257B and 5017B charge amplifier. The main intention was to compare the profiles of forces and related currents for different combinations of machining parameters. Subsequent analyzes of those signals, i.e., F_Z with I_Z, and resultant cutting force F_R with I_{MS}, have expectedly revealed high analogy of compared types of signals (Fig. 2.).

The experiment is characterized with the following features:

-- two medical drills of the same geometry, material type and diameter (4.5 mm), but with two different cutting edges conditions (Fig. 3) – Sharp Drill (SD) and Worn Drill (WD);

-- 12 combinations of cutting speeds (10; 30; 50 m/min), and feed rates (0.01; 0.03; 0.05; 0.1 mm/rev) – cutting speeds correspond to spindle speeds of 707.4 rpm, 2122.1 rpm and 3536.8 rpm, respectively;

-- each combination of machining parameters were randomly repeated 10 times for both medical drills;

-- fresh bovine tibia with average diaphysis cortical thickness (drilling depth) of 8.5 mm.

B. Signal Processing and Tool Wear Features Extraction

All signals were measured with 1 ms sampling rate. Raw measured signals have been analyzed in frequency domain using Fast Fourier Transform (FFT) algorithm. Based on that analyzes, and before extracting features from time domain, signals were filtered using the fifth-order low-pass Butterworth filter with a cutoff frequency of 2 Hz (Fig. 4). After that, 6 types of features were extracted from filtered signals (first 6 features from Table I).

First two features were maximum values of both types of current signals (*Max_I*$_Z$, *Max_I*$_{MS}$). In the case of I_Z, the direction of Z-axis movement was negative, so *Max_I*$_Z$ has been determined using absolute current values. They were calculated based on an average value of the 10% of the highest current values, thus neutralizing eventual occurrence of transient spikes (Fig. 5).

The next two features (*Area_I*$_Z$, *Area_I*$_{MS}$) were areas under current curves between time T_1 - start of drilling, and T_2 - end of cortical bone drilling (Fig. 5).

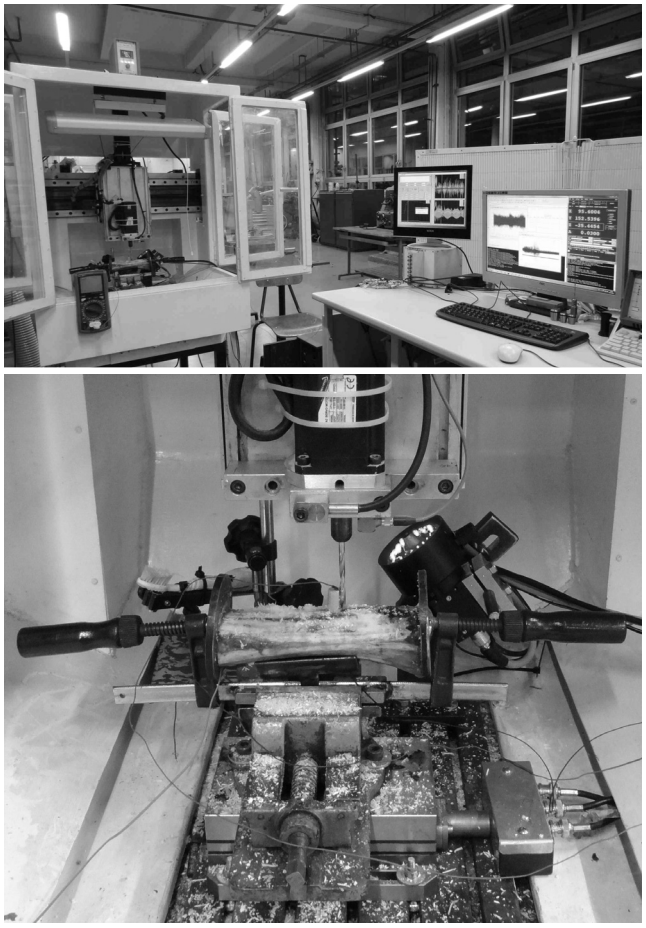

Fig. 1. Experimental setup

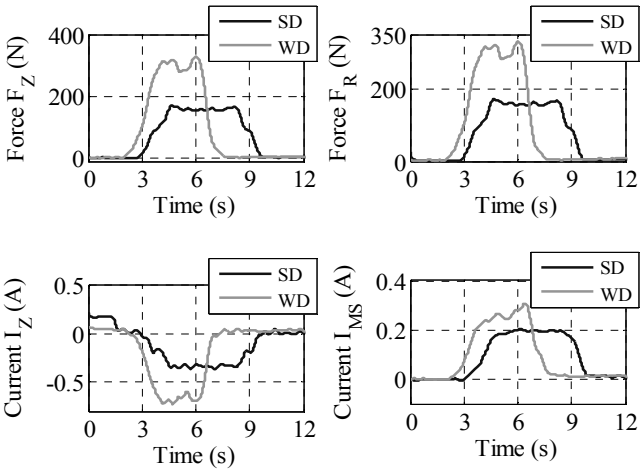

Fig. 2. Comparison of filtered force and current signals

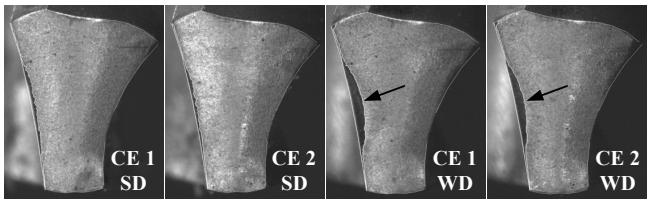

Fig. 3. Images of both cutting edges (CE1, CE2) after drilling with sharp drill (SD) and worn drill (WD) with observable (arrow pointing to) flank wear zone

ISBN: 978-988-19252-7-5
ISSN: 2078-0958 (Print); ISSN: 2078-0966 (Online)

TABLE I
LIST OF DRILL WEAR FEATURES

Feature	Description
Max_I_Z	Average of a group of 10% highest absolute I_Z current values obtained from feed motor drive (vertical or Z-axis)
Max_I_{MS}	Average of a group of 10% highest I_{MS} current values obtained from main spindle motor drive
Area_I_Z	Area under the I_Z=f(time) curve
Area_I_{MS}	Area under the I_{MS}=f(time) curve
Area_P_I_z	Area under the P_Z=f(time) curve (P_Z is Z-axis motor power)
Area_P_I_{MS}	Area under the P_{MS}=f(time) curve (P_{MS} is main spindle motor power)
P_RF_I_{MS}	Power of rotational frequency component of the I_{MS} signal
P_CEF_I_{MS}	Power of cutting edges frequency component of the I_{MS} signal

The remaining two features from the time domain (*Area_P_I_Z*, *Area_P_I_MS*) were areas under the motor power curve for Z-axis and main spindle. They were very similar to the previous two, in a way that they represent a sort of "weighted" *Area_I_Z* and *Area_I_MS* since

$$P_Z = K_T I_Z \omega_Z \text{ and } P_{MS} = K_T I_{MS} \omega_{MS}, \quad (10)$$

where K_T is motor torque constant (K_T = 0,46 Nm/A), while ω_Z and ω_{MS} are angular velocities of Z-axis feed drive and main spindle, respectively.

As for the features from the frequency domain, power of spectral components related to the rotation frequency (RF) and cutting edges frequency (CEF) were chosen [12]. Since drill has two cutting edges, CEF was twice as high as RF. Those features were obtained using the FFT algorithm. Subsequent analyzes of FFT spectrum of signals, related to different combinations of chosen machining parameters, have shown dominant spectral components on RF and CEF in mostly main spindle current signals. This was usually not the case with I_Z signals, as shown in Fig. 6. Therefore, power of spectral components on RF and CEF of just main spindle drive currents (*P_RF_I_MS* and *P_CEF_I_MS*) have been finally taken into consideration for drill wear classification in this experiment. In most samples, power of spectral components on the RF was higher than the one on CEF.

IV. RESULTS OF CLASSIFICATION

With 12 combinations of machining parameters, 10 measurements for each combination and two drill wear levels (classification groups), 240 sets of data or samples were collected in total. Half of them were used in the learning phase, and the rest in the testing phase of the RBF NN classifier. In other words, 5 out of 10 samples of repetitive measurements for each combination of machining parameters were used in the learning phase, and the remaining five participated in the formation of 5 test sets.

In order to analyze applicability of chosen tool wear features and to find combination(s) which provide the best classification performance, learning/testing procedure was divided into several steps. In the first step, every feature has been analyzed separately, and the results are presented in Table II in the form of the percentage of accurately

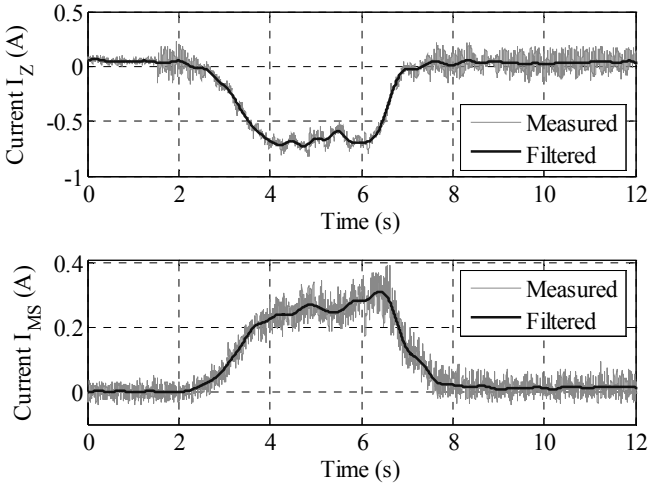

Fig. 4. Measured (raw) and filtered current signals

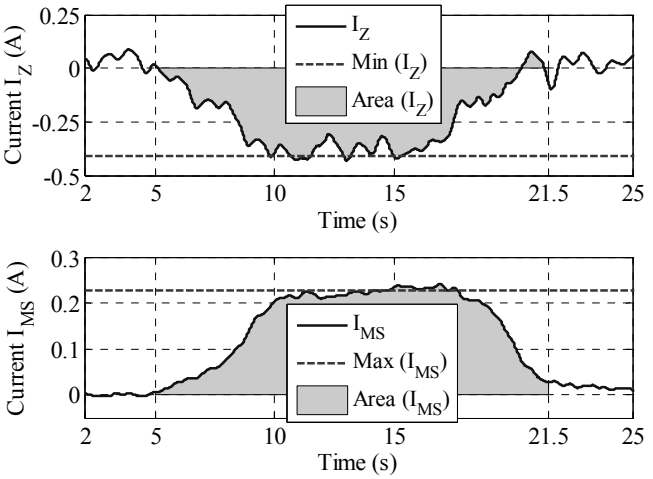

Fig. 5. Determination of extreme current values and area under curves between start (T_1) and end of cortical bone drilling (T_2) – in this example T_1=5s and T_2=21.5s

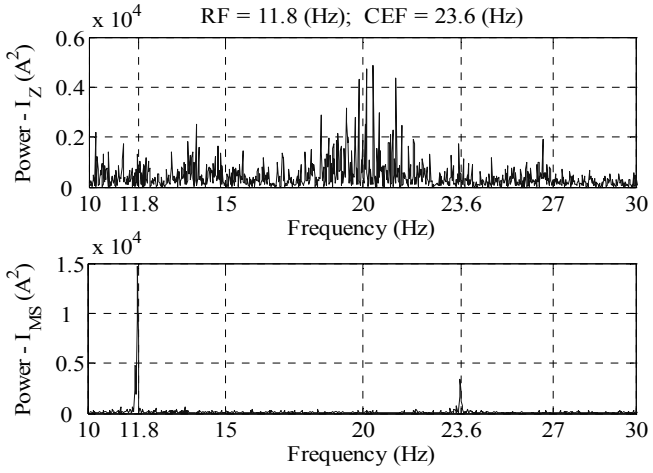

Fig. 6. Power spectrum of I_Z and I_{MS} signals – in this example n = 707.4 rpm → RF = 11.8 Hz → CEF = 2*RF = 23.6 Hz

classified samples. These results were obtained using full RBF NN hidden layer structure (120 neurons), i.e., with β_C=0 (the number of hidden layer neurons were equal to the number of learning samples). It should be also mentioned here that all presented results in this paper were achieved using cutting speed and feed rate as two additional NN inputs, and that classification success rate in the learning

ISBN: 978-988-19252-7-5
ISSN: 2078-0958 (Print); ISSN: 2078-0966 (Online)

phase was 100%.

The results have shown that extreme current values (Max_I_Z and Max_I_{MS}) have individually achieved the highest classification precision. The rest of features managed to correctly classify 60-65% of samples, with the lowest success rate accomplished by the features from the frequency domain ($P\_RF\_I_{MS}$ and $P\_CEF\_I_{MS}$).

Based on these first results, further analyzes of different tool wear feature combinations have been performed, again using full hidden layer structure (β_C=0). Feature combinations have generally and expectedly achieved higher classification accuracy than the individual features (Table III). Combination of extreme current values (I1, I2) achieved the highest classification accuracy (94.2%). Three more combinations accomplished success rate over 90%, mostly due to the influence of I1 and I2.

For those four combinations additional tests have been performed in the sense of finding the lowest RBF NN hidden layer structure ($\beta_C \neq 0$) which is able to provide close to or maybe even better results than the one achieved with full hidden layer structure. Results are presented in Table IV.

TABLE II
CLASSIFICATION RESULTS OF INDIVIDUALLY TESTED FEATURES (WITH $\beta_C = 0$) – ACCURATELY CLASSIFIED SAMPLES, (%)

Feature	TEST					
	T1	T2	T3	T4	T5	Avg.
(I1) Max_I_Z	70.8	75.0	75.0	79.2	83.3	76.7
(I2) Max_I_{MS}	79.2	91.7	83.3	91.7	95.8	88.3
(I3) $Area\_I_Z$	62.5	62.5	66.7	66.7	70.8	65.8
(I4) $Area\_I_{MS}$	45.8	54.2	45.8	70.8	75.0	58.3
(I5) $Area\_P\_I_z$	62.5	62.5	62.5	66.7	70.8	65.0
(I6) $Area\_P\_I_{MS}$	54.2	58.3	50.0	62.5	70.8	59.2
(I7) $P\_RF\_I_{MS}$	70.8	45.8	50.0	58.3	58.3	56.7
(I8) $P\_CEF\_I_{MS}$	54.2	54.2	41.7	45.8	41.7	47.5

TABLE III
CLASSIFICATION RESULTS OF FEATURE COMBINATIONS (WITH $\beta_C = 0$) – ACCURATELY CLASSIFIED SAMPLES, (%)

Feature	TEST					
	T1	T2	T3	T4	T5	Avg.
I1, I2	91.7	95.8	91.7	95.8	95.8	94.2
I3, I4	70.8	54.2	70.8	75.0	75.0	69.2
I5, I6	70.8	50.0	66.7	66.7	75.0	65.8
I1, I2, I3, I4	87.5	91.7	91.7	91.7	95.8	91.7
I1, I2, I5, I6	70.8	83.3	91.7	91.7	91.7	85.8
I7, I8	62.5	50.0	45.8	54.2	50.0	52.5
I1, I2, I7, I8	95.8	95.8	87.5	91.7	87.5	91.7
I1, …, I4, I7, I8	91.7	91.7	91.7	87.5	95.8	91.7
I1, …, I8	79.2	87.5	87.5	87.5	91.7	86.7

TABLE IV
CLASSIFICATION RESULTS OF CHOSEN FEATURE COMBINATIONS (WITH $\beta_C \neq 0$) – ACCURATELY CLASSIFIED SAMPLES, (%)

Feature	TEST					
	T1	T2	T3	T4	T5	Avg.
I1, I2	91.7	91.7	91.7	95.8	95.8	93.3
I1, I2, I3, I4	83.3	91.7	87.5	91.7	95.8	90.0
I1, I2, I7, I8	95.8	91.7	87.5	91.7	87.5	90.8
I1, …, I4, I7, I8	91.7	91.7	87.5	83.3	91.7	89.2
I1, I2	4-96-2 (no. of input - hidden - output layer neurons)					
I1, I2, I3, I4	6-108-2					
I1, I2, I7, I8	6-107-2					
I1, …, I4, I7, I8	4-101-2					

V. CONCLUSION

The results of this preliminary research study suggest good potential of servomotor current signals in medical drill wear monitoring. Considering the chosen type of drill, machining parameter combinations and bone characteristics, extreme current values of main spindle and feed drives have shown the highest sensitivity to variations of drill wear level. The remaining features from the time and frequency domain did not accomplish such high classification accuracy when analyzed individually or in mutual combinations.

However, areas under the motor current and power curves are expected to be among the dominant features in drilling temperature classification. This type of features is closely related to the total amount of electric energy used in the cutting process, whose large portion is transformed into heat energy which causes temperature rise and possible thermal osteonecrosis.

Extension of presented model with the critical drilling temperature identification is planned to be performed in the next part of this study. Further analyzes will also include model extensions with new types of tool wear and drilling temperature features extracted from vibration and acoustic emission sensors.

REFERENCES

[1] G. Augustin, T. Zigman, S. Davila, T. Udiljak, T. Staroveski, D. Brezak, and S. Babic, "Cortical bone drilling and thermal osteonecrosis," *Clinical Biomechanics*, vol. 27, no. 4, pp. 313-325, May 2012.

[2] S. Karmani, "The thermal properties of bone and the effects of surgical intervention," *Current Orthopaedics*, vol. 20, no. 1, pp. 52-58, Feb. 2006.

[3] L. S. Mathews and C. Hirsch, "Temperature measured in human cortical bone when drilling," *The Journal of Bone Joint Surgery*, vol. 54, no. 2, pp. 297-308, Apr. 1972.

[4] G.E. Chacon, D.L. Bower, P.E. Larsen, E.A. McGlumphy, and F.M. Beck, "Heat Production by 3 Implant Drill Systems After Repeated Drilling and Sterilization", *Journal of Oral and Maxillofacial Surgery*, vol. 64, no. 2, pp. 265-269, Feb. 2006.

[5] T. P. Queiroz, F. Á. Souza, R. Okamoto, R. Margonar, V. A. Pereira-Filho, I. R. Garcia, and E. H. Vieira, "Evaluation of Immediate Bone-Cell Viability and of Drill Wear After Implant Osteotomies: Immunohistochemistry and Scanning Electron Microscopy Analysis," *Journal of Oral and Maxillofacial Surgery*, vol. 66, no. 6, pp. 1233-1240, Jun. 2008.

[6] R. M. Jochum and P. A. Reichart, "Influence of multiple use of Timedur® – titanium cannon drills: thermal response and scanning electron microscopic findings," *Clinical Oral Implants Research*, vol. 11, no. 2, pp. 139-143, Apr. 2000.

[7] J. Singh, J.H. Davenport, and D.J. Pegg, "A national survey of instrument sharpening guidelines," *The Surgeon*, vol. 8, no. 3, pp. 136-139, Jun. 2010.

[8] S.R.H. Davidson, "Heat transfer in bone during drilling," M.S. Thesis, Institute of Biomaterials and Biomedical Engineering, University of Toronto, Canada, 1999.

[9] JuEun Lee, Yoed Rabin, and O. Burak Ozdoganlar, "A new thermal model for bone drilling with applications to orthopaedic surgery," *Medical Engineering & Physics*, vol. 33, no. 10, pp. 1234–1244, Dec. 2011.

[10] E. Jantunen, "A summary of methods applied to tool condition monitoring in drilling," *International Journal of Machine Tools & Manufacture*, vol. 42, no. 9, pp. 997-1010, Jul. 2002.

[11] B. Novakovic, D. Majetic, and M. Siroki, *Artificial Neural Networks.* Zagreb: University of Zagreb, Faculty of Mechanical Engineering and Naval Architecture, 1998.

[12] P.W. Prickett and C. Johns, "An overview of approaches to end milling tool monitoring," *International Journal of Machine Tools & Manufacture*, vol. 39, no. 1, pp.105-122, Jan. 1999.

ISBN: 978-988-19252-7-5
ISSN: 2078-0958 (Print); ISSN: 2078-0966 (Online)